Pergamon

PII: S0306-4522(00)00382-1

www.elsevier.com/locate/neuroscience

Neuroscience Vol. 101, No. 2, pp. 403–416, 2000

0306-4522/00 $20.00+0.00

IDENTIFICATION OF CELL TYPES IN BRAIN SLICES OF THE INFERIOR COLLICULUS

D. PERUZZI,* S. SIVARAMAKRISHNAN and D. L. OLIVER†

Department of Neuroscience, University of Connecticut Health Center, Farmington CT 06030-3405, USA

Abstract—Different type neurons in the inferior colliculus may have different functions. Recent intracellular studies of the inferior colliculus suggest that intrinsic electrical properties contribute to discharge patterns, but the intrinsic discharge patterns have not been fully characterized in the central nucleus, the main part of the inferior colliculus. Whether different types of neurons are related to different discharge patterns is unclear.

We have used intracellular and whole-cell patch clamp-recording techniques in a brain slice preparation to better characterize discharge patterns and cell types in the central nucleus. Several types of discharge pattern were found in the inferior colliculus in response to long pulses of intracellular depolarizations. Rebound and buildup–pauser discharges, together, comprise neurons with a sustained response and are the majority of the neurons in the inferior colliculus. Both of these types of discharge pattern could be adapting or regular. Onset discharges distinguished another group of neurons. Onset neurons can also entrain to higher frequency stimuli than sustained neurons. Discharge patterns are correlated with distinctive current–voltage relationships and with some aspects of dendritic morphology. However, the morphological data demonstrates that the discharge patterns do not correspond simply to disc-shaped (flat) or stellate (less-flat) categories.

This is the first extensive analysis of electrophysiological properties of the central nucleus of the inferior colliculus *in vitro*. We suggest that there may be at least three functional classes of neurons and have implications for signal processing in the inferior colliculus.

Key words: auditory pathways, temporal coding, rat, discharge patterns, neuronal morphology.

What are the neuron types in the inferior colliculus (IC), the principal part of the auditory pathway in the midbrain? Morphology suggests the central nucleus of the IC should have two types of neurons based on the shape and orientation of the dendritic tree.[9,22,25,33,51] The principal neuron is disc-shaped (called the flat neuron in rats) with dendrites that parallel the fibro-dendritic laminae. A second, less common neuron with a different dendritic morphology is also found in all species studied (e.g. the less-flat neuron in the rat).

In contrast, physiology suggests three or more cell types are present based on responses to binaural acoustic stimuli and frequency-amplitude maps.[6,13,45] Morphological classification based on dendritic shape or orientation is reconciled with some physiological characteristics and not others. For example, neurons with similar binaural properties often have heterogenous morphology, indicating a lack of correlation, whereas the presence of inhibitory side bands is well correlated with stellate morphology.[18]

The discharge patterns in the IC may be a useful method to classify neurons. Onset, sustained, buildup, and pauser discharge patterns are well-documented in many species (e.g. cat,[19] rabbit,[17] guinea-pig,[20,46] gerbil,[53] and rat[36]). In the cochlear nucleus, discharge patterns correlate well with specific morphological cell types.[35,49,50] Efforts to characterize the intrinsic electrical properties of IC neurons are, however, just beginning[21,58,59] and discharge patterns have not been correlated with morphology. A more detailed analysis is needed to test the hypothesis that cell types are indicated by discharge pattern, and whether functionally defined cell types are correlated with other morphological properties such as Nissl pattern, cell body size or shape, dendritic branching, dendritic spines, or synaptic distribution.

The present study examines the discharge patterns of neurons in brain slices from the IC of the rat. In order to clearly distinguish the intrinsic discharge pattern of the cell, we use intracellular stimulation rather than synaptic inputs. The first part of the study defines the cell type based on discharge patterns during long current injections that allow the analysis of firing variance, adaptation, and dynamic range. The second part examines the correlation of the discharge pattern to temporal processing and current–voltage relationships.

EXPERIMENTAL PROCEDURES

Intracellular sharp microelectrode recordings

Slices through the IC were prepared from Long–Evans hooded rats (Charles River) according to previously published methods.[55] Male or female rats were used under NIH and institutional animal care guidelines, and all efforts were made to minimize animal suffering, to reduce the number of animals used, and to utilize alternatives to *in vivo* techniques if available. Rats were a mean age of 25.8 days (range 14–44 days) and weight of 78.2 ± 36.2 g (mean ± S.D.). Animals were anesthetized with a mixture of ketamine (97.5 mg/ml) and xylazine (2.43 mg/ml, 0.1 ml of mixture per 100 g body weight, intramuscular) to a level at which they did not respond to a brisk toe pinch. Rats were perfused through the heart with cold (~4°C), modified cerebral spinal fluid (CSF) where the external NaCl was substituted with an iso-osmotic concentration of sucrose (in mM: KCl, 5.0; $MgSO_4$, 1.3; KH_2PO_4, 1.2; $CaCl_2$, 2.4; $NaHCO_3$, 26; dextrose, 10; sucrose, 240) saturated with 95% O_2/5% CO_2 gas.[2] Immediately after perfusion, the head was removed, placed in cold, oxygenated modified CSF,

*Current address: Department of Neuroscience, New York Institute of Technology, New York College of Osteopathic Medicine, Old Westbury, NY 11568, USA

†To whom correspondence should be addressed. Tel.: +1-860-679-2241; fax +1-860-679-8766.

E-mail address: doliver@neuron.uchc.edu (D. L. Oliver).

Abbreviations: CSF, cerebral spinal fluid; CV, coefficient of variation; EGTA, ethyleneglycolbis(aminotheyl ether)tetra-acetate; IC, inferior colliculus; ITD, interaural temporal difference; TTX, tetrodotoxin.

and the dorsal aspect of the cerebellum and caudal cerebrum were quickly exposed. Parallel cuts, roughly perpendicular to the long axis of the brainstem, were made at the caudal border of the mesencephalon and rostrally, through the middle of the superior colliculus. The tissue block was attached to a chuck with cyanoacrylate glue (Wood and Leather Krazy Glue; Borden, Inc, Columbus, OH) and cut into 300 μm slices with a Vibratome (Lancer) in cold, oxygenated modified CSF. At this point, slices were made in either the transverse plane, or in a plane roughly parallel to the fibrodendritic laminae of the central nucleus of the IC. For the latter process, an additional cut was made parallel to the layers so that when the resulting tissue block was glued to the chuck, slices would be cut in the laminar plane. Laminar slices preserved the dendrites in the layers of the IC.

Slices were placed in an interface brain-slice chamber (Medical Systems, Greenvale, NY) and maintained initially at room temperature in a continuous flow of moist gas (95% O_2; 5% CO_2) and a 1:1 mixture of oxygenated, modified CSF and artificial CSF with normal sodium (CSF, in mM: KCl, 5.0; $MgSO_4$, 1.3; KH_2PO_4, 1.2; $CaCl_2$, 2.4; $NaHCO_3$, 26; dextrose, 10; NaCl, 120). After 10–15 min, the slices were gradually heated to 33.5°C and perfused with CSF containing normal sodium. Recordings were made at least 1 h after the slices reached 33.5°C.

Recordings were made with sharp, intracellular electrodes and digitized online. Electrodes were pulled from 1.0 mm borosilicate glass on a P-80/P.C. Flaming Brown Micropipette Puller (Sutter Instrument Co., Novato, CA). Electrodes had a resistance of 90–150 MΩ and were filled with 2% neurobiotin (Vector, Burlingame, CA) in 2 M potassium acetate. Electrodes were advanced with a piezoelectric microdrive (Burleigh Instruments, Fishers, NY). Electrophysiological data were digitized for on-line and off-line analysis. Data were collected with a Neurodata amplifier and a Lab Master DMA (Scientific Solutions Inc., Solon, OH) at a 12 kHz sampling rate controlled by custom software (Icepac II, L. Haberly, University of Wisconsin).

Current injections between −1.0 and +1.0 nA were used to elicit voltage changes in the IC neurons. To determine the discharge pattern, a 300 ms current between +0.1 and +1.0 nA (0.1 nA increments) was injected. Regularity of firing was analysed in two ways. A neuron was considered regular (no adaptation) if none of its interspike intervals exceeded twice the first interspike interval. Coefficients of variation were calculated by dividing the standard deviation of interspike intervals by the mean interspike intervals. Off-responses were examined after 300 ms injections of current between −0.1 and −1.0 nA (0.1 nA steps). Rebound was identified as a large, slow depolarizing response upon offset of hyperpolarizing current. This rebound depolarization rose above the initial resting potential measured before hyperpolarization and was independent of the presence of action potentials. Buildup and pauser behavior was determined by the application of hyperpolarization prior to depolarization. Prehyperpolarizations (300 ms for patch electrodes, seconds for sharp electrodes) used sufficient current to hyperpolarize the neuron −5 to −20 mV below resting potential (−0.1 to −0.5 nA). A delay in the onset of firing or a pause in firing (greater than approximately twice the average interspike interval) indicated buildup–pauser behavior. Trains were made up of short current injections (less than 1 ms) at varying frequencies whose amplitude was adjusted to just above threshold for one action potential. A neuron was considered to have failed to follow a train when one action potential was missed.

Whole-cell patch-clamp recordings

We also used the whole-cell patch clamp technique to record from IC neurons.[11] Younger rats, between 8 and 17 days old, were used in these experiments. Following anesthesia with ketamine/xylazine, the brain was removed and placed in warm (35°C), oxygenated normal CSF and a block containing the IC was glued onto the stage of a vibratome (Lancer/TPI, O'Fallon, MO). Transverse brain slices, 300-μm-thick, were cut through the IC and incubated at 35°C in saline oxygenated with a 95% O_2/5% CO_2 mixture for an hour before recordings were made. For recording, individual slices were transferred to a microscope-mounted, Peltier-driven slice chamber (model PSMI, Medical Systems, Greenvale, NY) and perfused with normal CSF at 33°C having the same composition as that used for the intracellular microelectrode recordings. Neurons were visualized with a ×40/.75NA water immersion objective and Nomarski optics on a fixed-stage microscope (Zeiss Axioskop). Current clamp recording techniques were used to examine the firing pattern of the cell. An EPC-8 amplifier (HEKA Elektroniks) and PClamp software (Axon Instruments, Foster City, CA) were used for data collection and analyses. Data were filtered at 5 kHz. Patch pipettes were pulled from borosilicate glass (Kimax-51, 1.5 mm O.D., 1.0 mm I.D.) and were 5–7 MΩ in resistance. Pipettes were filled with a solution containing, in mM: 120 K Gluconate, 5 NaCl, 11 EGTA, 1 $CaCl_2$, 0.3 Na-GTP, 10 HEPES, pH 7.3. Lucifer Yellow (dipotassium salt, 0.3%; Sigma, St. Louis, MO) was added to the internal solution during some of the recordings. To block sodium channels, 1 μM tetrodotoxin (TTX; Sigma, St. Louis, MO) was perfused with the normal CSF.

Anatomical methods

Some neurons were injected with neurobiotin through sharp electrodes (+0.5–2.0 nA, 200 ms pulses, 50% duty cycle, 8–12 min) or were filled with Lucifer Yellow from patch pipettes. Slices that contained neurobiotin- or Lucifer Yellow-filled neurons were fixed for at least one day in buffered formyl saline (3.6% paraformaldehyde in 0.1 M phosphate buffer/0.9% NaCl, pH 7.4). Whole slices containing neurons labeled with Lucifer Yellow were mounted in a 2.5% solution of 1,4-diazobicyclo-[2.2.2]-octane (Aldrich, Milwaukee, WI) in a 9:1 mixture of glycerin/phosphate buffer (pH 8.6) to retard photobleaching. Slices containing neurobiotin-filled cells were cryoprotected in 30% sucrose (buffered formyl saline) overnight, and sectioned on a sliding microtome at 60 μm. To visualize the neurons, avidin–biotin-peroxidase complex histochemistry (1:200, overnight, Vector, Burlingame, CA) was preceded by 0.5% H_2O_2 (20 min), 0.1 M phosphate buffer rinse (5 min), and detergent rinse (15 min, 0.1% Triton X-100). The next day following rinses and preincubation in 0.05% diaminobenzidine (15 min), the sections were incubated in 0.05% diaminobenzidine with 0.01% H_2O_2 for 17.5 min.[1] Finally, sections were dried onto slices, dehydrated in ethyl alcohols, cleared in Histoclear (National Diagnostics, Atlanta, GA), and coverslipped in Permount (Fisher, Pittsburgh, PA). Additional slices without injected cells were also fixed, sectioned, and Nissl-stained with Cresyl Violet.

Neurons were reconstructed in three dimensions on a Zeiss Axioskop with a ×40/1.0NA or ×63/1.25NA lens and an integrating video camera (Dage 72) that was interfaced to a computer system with neuroanatomical reconstruction software (Neurolucida, Microbrightfield, Burlington, VT). Since neurobiotion filled neurons had undergone dehydration, shrinkage correction factors were estimated and applied. Lucifer Yellow cells were imaged with epi-fluorescent illumination. The perimeter, area, and average diameter of the cell body were estimated from the Neurolucida reconstructions and, in the case of Lucifer Yellow-filled neurons, from digital images taken at the time of filling. The length of the dendritic tree was the maximum length in any axis. The axis of the maximum length was taken to be the vector of orientation. The width of the dendritic tree was the narrowest dimension perpendicular to the axis of the dendritic length. These estimates generally follow the quantitative methods of Malmierca *et al.*[22] that define types of neurons in the IC of the rat.

RESULTS

Fifty-eight neurons were studied with sharp electrodes and 41 neurons were studied with patch electrodes. These neurons were found throughout the IC. In experiments using sharp electrodes, 46/58 neurons were located in the central nucleus of the IC as defined by Faye-Lund and Osen.[7] The remaining 12 were studied in the rostral IC that contains several subdivisions, the intercollicular tegmentum, commissural nuclei, brachium of the IC, and remnants of the central nucleus. It corresponds to the rostral portion of external cortex.[7] The majority of neurons studied with patch electrodes ($n = 41$) were also in the central nucleus with additional neurons in the external and dorsal cortex.

We examined 52 neurons in the IC that were labeled by intracellular injection of neurobiotin (sharp electrodes, $n = 18$) or filled with Lucifer Yellow (patch electrodes, $n = 34$). Results for neurobiotin-filled and Lucifer Yellow-filled neurons were the same even though the Lucifer Yellow results were obtained from neurons 10–14 days of age. In

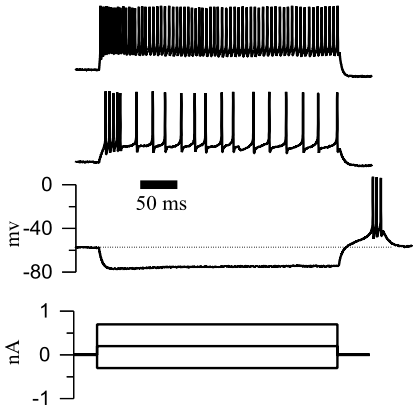

Fig. 1. Rebound neurons (15/58 sharp electrodes, 14/41 patch electrodes) are distinguished by a large depolarization upon offset of hyperpolarizing current injection. Rebound neurons have a sustained pattern of action potentials (two top traces) in response to depolarizing current injections. A large depolarization with a cluster of action potentials riding on top (third trace) at the offset of a hyperpolarizing current injection is characteristic of rebound neurons. This rebound never occurs in buildup-pauser (Fig. 4A, third trace) or onset (Fig. 8, fourth trace) neurons (dotted line indicates the resting membrane potential).

general, the most detailed morphological observations were limited to the best-filled neurons ($n = 26$) where there was a substantial amount of filled dendritic tree and unambiguous physiological results. Most of the filled neurons were located in the central nucleus, but at least 10 well-filled cells were in the external cortex or rostral IC. However, the location of the neuron did not predict the physiological response (see below). Neurons with different discharge patterns (see below) were found in each sub-division of the IC studied in roughly equal proportions. Therefore, the discharge pattern did not predict the location of the neuron in the IC.

All but a few cells (indicated below) were disc-shaped in that their dendritic fields appeared to be parallel to the fibrodendritic laminae of the central nucleus. Most injected neurons in the central nucleus were 'flat' (dendritic fields < 70 μm at the narrowest dimension) when rotated in 3D. Three cells with less-flat dendritic trees were an exception and indicate that the flat and less-flat designations did not correspond to neurons with unique discharge behaviors (see below: one buildup–pauser, one rebound, one onset).

Discharge patterns

Neurons were characterized based on their responses to long (300–600 ms) injections of depolarizing current, their response at offset to a hyperpolarizing current injection, and the effects of injections of hyperpolarizing current before the depolarizing stimulus. Neurons had either sustained or onset discharges.

Sustained

Most neurons in the IC had sustained discharges to depolarizing currents (41/58, 71%, sharp electrodes; 27/41, 66%, patch electrodes). Neurons with sustained discharges could be further subdivided as those with a depolarizing, offset rebound, those with buildup–pauser behavior, and those with neither. Only 5/58 (9%, sharp electrodes) and 5/41 neurons (12% patch electrodes) had sustained discharges but lacked rebound or buildup–pauser behaviors.

Rebound response

The hallmark of the rebound response was a large, slow depolarizing off-response to hyperpolarizing current injections (Fig. 1). The rebound was similar to a Ca^{++}-based rebound potential described previously in the dorsal cortex of the IC.[55] These neurons had sustained firing to depolarizing currents. The slow rebound was not seen in buildup–pauser neurons (Fig. 4) or in onset neurons (Fig. 8, see also Fig. 11A). However, all neurons could show Na^{+}-based action potentials at offset. In the case of the rebound neuron, the Na^{+} spikes rode on top of the rebound depolarization (see Figs 2 and 3). Rebound neurons had firing patterns to depolarization that were not changed by pre-hyperpolarization (sharp electrodes, $n = 9$). Rebound behavior was seen in 15/58 (26%) neurons studied with sharp electrodes and 14/41 (34%) neurons studied with patch electrodes.

Injected neurons with a rebound firing pattern were a heterogeneous group that was characterized by complex, highly branched dendritic trees. In the central nucleus, neurons with rebound discharges had flat, disc-shaped dendritic fields ($n = 5$; Fig. 2A, B). A neuron in caudal cortex ($n = 3$; Fig. 2C) was similarly oriented with a smaller, less-flat (>70 μm thick) dendritic field. Neurons in external cortex were both large and small and could be pyramidal or stellate ($n = 3$; not shown). Thus, all rebound neurons did not have a dendritic field with the same shape (flat, less-flat, stellate). Rebound neurons often had filled local axons (Fig. 3). Somatic areas and somatic diameters in the central nucleus and dorsal cortex were often larger in rebound cells than buildup–pauser neurons (mean areas and diameters: rebound, 232 μm^2, 17 μm, $n = 10$; buildup–pauser, 184 μm^2, 15 μm, $n = 5$).

Buildup–pauser response

Buildup–pauser neurons had their discharge pattern altered when the depolarizing stimulus was preceded by a hyperpolarizing injection of current (Fig. 4). In other words, a sustained response was changed to a buildup or a pauser response. This behavior is similar to the "buildup" response in the cochlear nucleus[42] that is caused by the A-type potassium current and also revealed by pre-hyperpolarization.[14,23] The sustained firing of one neuron is shown at two current levels (Fig. 4A). This neuron was pre-hyperpolarized by application of seconds-long hyperpolarizing current before the 300 ms depolarizing current injection (Fig. 4B). Pre-hyperpolarization caused the responses to change. At the smaller current level, the first spike became delayed. Instead of spiking at the onset of the depolarizing current pulse, the membrane potential "built up" from below threshold at the start of the depolarizing pulse to above threshold about 50 ms after the beginning of the depolarizing current pulse. In response to a larger depolarizing current, the first spike occurred at shorter latency, but there was a pause between the first and second spikes, a "pauser" pattern. Thus, the buildup and pauser effects were both caused by the pre-hyperpolarization, and the buildup changed to a pause when the neuron was depolarized to a greater extent. Some of the most sensitive neurons were affected by hyperpolarizations as little as 10 mV below resting membrane potential. Prehyperpolarization caused a change to buildup–pauser in 7/24 (29%) neurons tested using sharp electrodes and in 8/41 recordings with patch electrodes (20%). Experiments performed with

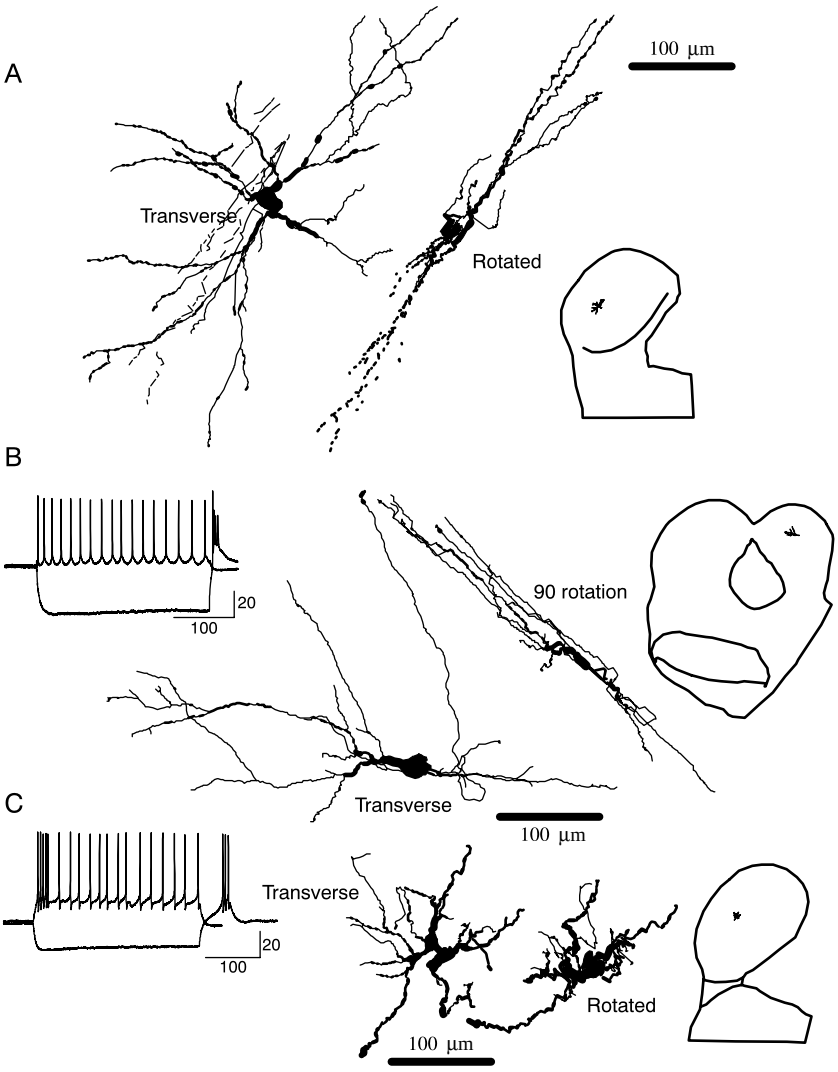

Fig. 2. Rebound neurons filled with neurobiotin. (A) Large neuron with flat field (60 μm) in the central nucleus (24 days old). (B) Large neuron with flat field (45 μm) in the central nucleus (18 days old). (C) Small neuron in caudal cortex or caudal central nucleus (37 days old). Physiology is seen on the left.

patch electrodes used 300 ms pre-hyperpolarization pulses and showed similar results (e.g. Fig. 5C, insert).

Injected neurons with buildup–pauser discharge patterns had dendrites that branched close to the soma ($n = 4$; Fig. 5). Proximal dendrites had fewer distal branches beyond that point. This gave rise to a simpler branching pattern, compared to the rebound cells, usually with eight or fewer dendrites at any point along the dendritic tree. Some buildup–pauser neurons were large (e.g. Fig. 5A) with disc-shaped dendritic fields that extended radially from the soma. Others were smaller (Fig. 5B). Some buildup–pauser neurons were oriented in the rostrocaudal direction at the border of the central nucleus and dorsal cortex (Fig. 5C). Thus, all neurons with the same firing pattern did not have one orientation.

Adaptation and regularity of firing in sustained neurons

Regular and adapting behavior was studied with sharp electrodes and seen in both buildup–pauser (5/7 regular and 2/7 adapting) and rebound (6/15 regular and 9/15 adapting) neurons. Regularity in sustained neurons was quantified by measurement of each interspike interval relative to the duration of the first interspike interval. Examples are plotted in Fig. 6. In neurons that displayed adaptation, interspike intervals increased throughout the current injection, and the increase was most pronounced at lower current levels (Fig. 6A). Other sustained neurons had interspike intervals that were no greater than twice the duration of the first interspike interval (Fig. 6B). Neurons that meet this criterion are "regular"[46] Buildup–pauser neurons could be adapting (Fig. 6A, BP) or regular (Fig. 6B, BP). In general, rebound neurons also displayed adapting (Fig. 6A, REB) or regular (Fig. 6B, REB) behavior. The adapting traces shown in Fig. 6A were typical of rebound neurons with adaptation in that interspike intervals increased 600% or more, more than the typical increase in buildup–pauser neurons.

A second method to quantify the amount of adaptation was calculation of the coefficient of variation (CV). The CV reflected regularity of interspike interval over the duration of the entire stimulus. Neurons with buildup–pauser responses tended to have lower CV values than neurons with rebound responses. Buildup–pauser neurons had CV values of 0.3 or less for most current levels (Fig. 6C). However, neurons with rebound behavior had higher mean CVs (> 0.4) especially at the intermediate current levels (0.5–0.7 nA). Thus, the rebound neurons showed greater

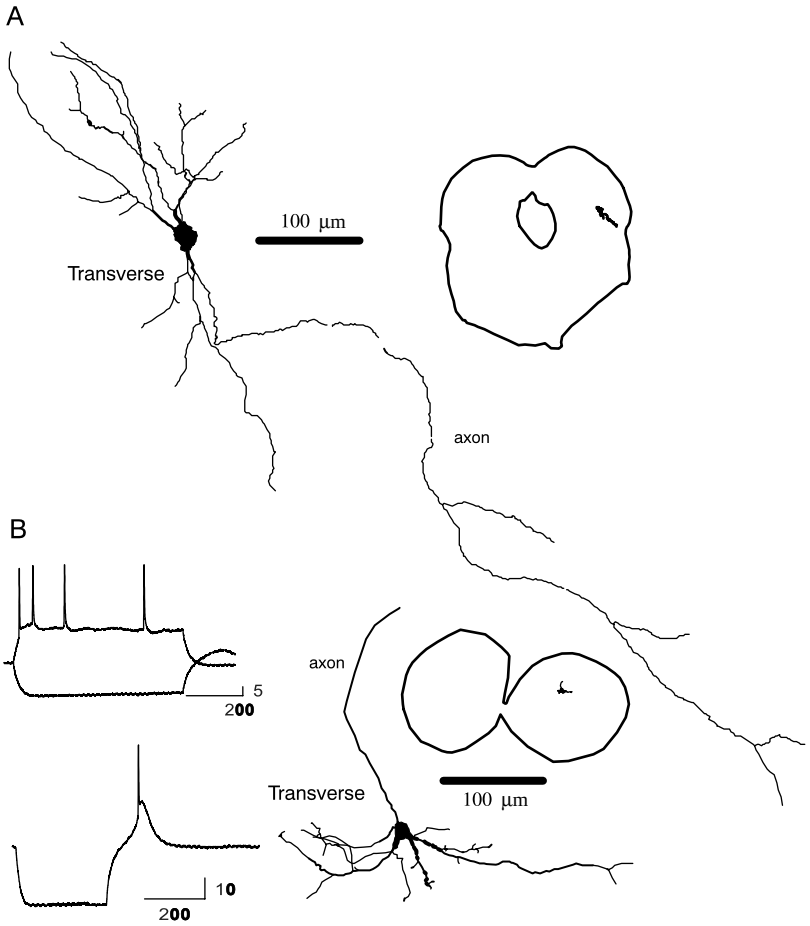

Fig. 3. Rebound neurons with filled axons. (A) Large, less-flat neuron (dendritic field width 80 μm at narrowest dimension) in the ventrolateral central nucleus with an axon that continues laterally into the vicinity of the lateral lemniscus (20 days old). B, Lucifer-Yellow-filled, flat neuron (50 μm) in central nucleus. The axon passes rostral and dorsal towards the dorsal cortex.

Table 1. Membrane properties of sustained and onset neurons (mean ± S.E.)

Firing pattern	*n*	RMP (mV)	AP threshold (mV)	AP amplitude (mV)
Sustained	41	− 59.3 ± 1.4	− 49.0 ± 1.25	60.95 ± 2.1
Onset	17	− 56.8 ± 2.1	− 46.4 ± 1.9	56.6 ± 2.3

Mean resting membrane potential (RMP), action potential (AP) threshold, AP amplitude.

adaptation, and the buildup–pauser neurons showed greater regularity.

Rate-level functions in sustained neurons

The rate-level functions as studied with sharp electrodes for buildup–pauser ($n = 7$) and rebound ($n = 8$) neurons are both very linear and are not significantly different from each other. When current level is plotted against spike-rate (Fig. 7A) the mean slopes (based on regression lines), indicating the change in rate per change in current, are similar: buildup–pauser, 221 ± 30 Hz/nA; rebound, 203 ± 14 Hz/nA. Some rebound neurons reached higher rates than buildup–pauser neurons. If the current and rate are both normalized to their greatest values for each neuron, the relationships become more tightly clustered (Fig. 7B). A student's *t*-test ($t = -1.75$, $df = 13$) showed no significant difference between slopes for buildup–pauser and rebound neurons.

Onset

Onset neurons were different from both buildup–pauser and rebound neurons in that their action potential pattern to long depolarizing injections was not sustained. Instead the pattern consisted of one or two action potentials at onset of depolarization (Fig. 8). Increasing the current level did not alter this behavior. The initial spiking activity was followed by a sustained depolarization which did not evoke further spikes. The onset response pattern was not an artifact of poor cellular health since these neurons had resting potentials, action potential height, and thresholds (Table 1) similar to sustained neurons. In onset cells, the time to reach 66% of instantaneous voltage was faster for depolarization than for hyperpolarization (1.27 ± 0.18 ms for 0.2 nA and 2.2 ± 0.2 ms for −0.2 nA). Moreover, the input resistances, measured at steady state and close to resting membrane potential, were higher than that of sustained neurons (see below).

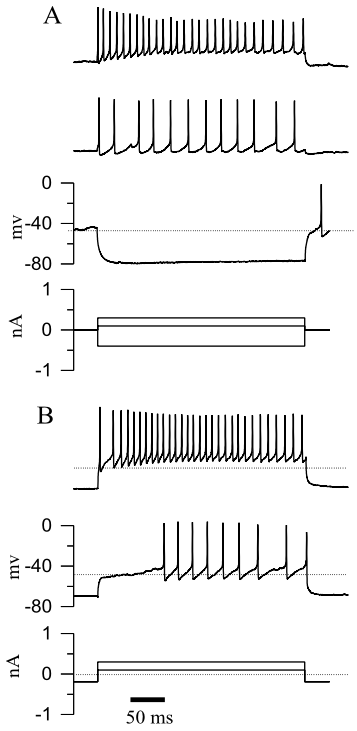

Fig. 4. Buildup-pauser neurons (7/24 sharp electrodes, 8/41 patch electrodes) have their discharge patterns changed when prehyperpolarized. (A) Buildup–pauser neurons have discharge patterns to depolarizing current injections that are sustained (two top traces). (B) The sustained pattern is changed to a buildup (second trace) or pauser (first trace) pattern when the depolarization is preceded by a hyperpolarizing current injection (dotted lines indicates voltage and current levels without prehyperpolarization).

Onset neurons had firing patterns to depolarization that were not changed by pre-hyperpolarization (sharp electrodes, $n = 4$). Onset discharges were seen in 17/58 (29%) neurons studied with sharp electrodes and in 14/41 (34%) neurons studied with patch electrodes.

Injected neurons with onset discharge patterns in the central nucleus had frequent dendritic branches (Fig. 9). The higher number of dendritic branches gave rise to a more 'complex' dendritic tree, as compared to the more sparsely branched dendritic tree of the buildup–pauser neurons. The dendritic field could be flat, less-flat, or stellate if the neuron was outside of the central nucleus. For onset cells in the rostral IC ($n = 2$, not shown), even higher numbers of branches were seen in the first 100 μm than in the central nucleus. Thus, onset cells could have more than one dendritic field shape.

Stimulus entrainment ability differed for onset and sustained neurons

Intrinsic electrical properties may be an important factor in creating the temporal response of IC neurons *in vivo*. Previous studies in the nucleus magnocellularis and medial nucleus of the trapezoid body[3,47] had used intracellular injections of short current pulse trains or sinusoidal currents to divorce the synaptically induced activity from the intrinsic properties of the cell. While these onset cells fire only once to a sustained current, they fire repeatedly to trains or sinusoidal currents. These studies suggested that the intrinsic membrane properties of onset neurons make them suitable for temporal coding.

To test the ability of IC neurons to code temporal information, we used a similar pulse-train protocol. Using sharp electrodes, we injected IC neurons with trains of short current pulses at different frequencies and measured their ability to entrain action potentials during the trains. Because the onset discharge was limited to one action potential at the beginning of a long depolarizing current pulse (Fig. 10A, top), we predicted that onset neurons in the IC might follow trains of short current pulses at a high rate. The result was that neurons with an onset discharge followed trains of short current pulses at high rates of up to 200 spikes/s (Fig. 10A, left middle). They failed to follow the pulse-trains at slightly higher rates (Fig. 10A, left bottom; 250 spikes/s). For an average of five onset cells, the maximum rate before failure was 114.8 ± 33.7 Hz. These results suggest that onset neurons may be adapted to respond to the temporal aspects of a stimulus.

By comparison, neurons with rebound responses could not respond to trains of short current pulses at high rates. For example, a rebound neuron (Fig. 10B, top) followed a train of short current pulses only at a slow rate (Fig. 10B, middle). It followed at a one-to-one ratio at a rate much lower (Fig. 10B, bottom) than the onset neuron (Fig. 10A, bottom). For a sample of sustained neurons, the maximum firing rate before failure was 39.3 ± 5.9 Hz ($n = 9$). These results suggest that IC neurons with sustained discharges may respond poorly to the temporal aspects of a stimulus.

Amplitude of after-hyperpolarizations differed for onset and sustained neurons

Another way in which onset neurons differed from sustained was that onset neurons had smaller after-hyperpolarizations. Using sharp electrodes, after-hyperpolarizations were studied in two ways. They were elicited after 300 ms hyperpolarizing current injections of 0.5 nA ($n = 38$) or by short (0.1–0.3 ms) pulses ($n = 13$). Hyperpolarizations after 300 ms pulses are smaller in onset neurons than in sustained neurons (1.4 ± 0.2 mV for onset vs. 5.5 ± 0.5 mV for sustained). The same is true when after-hyperpolarizations were measured after short stimuli (0.15 ± 0.3 mV for onset vs. 1.6 ± 0.7 mV for sustained).

Inward and outward rectification

To characterize the inward rectification of IC neurons, we used the whole-cell patch clamp technique. Patch electrodes passed current more easily than sharp electrodes and therefore proved to be a better tool to examine inward rectification in response to large amplitude hyperpolarizations. In addition to looking at inward rectification, firing patterns to depolarizing current injections were confirmed to be similar to those observed with sharp electrodes.

IC neurons exhibited active membrane properties during hyperpolarization. Hyperpolarizing current injections into the soma of IC neurons caused an inward rectification of the membrane potential (Fig. 11). Inward rectification was present in all IC cells, although its time-course and threshold varied. In all three cell types, some neurons developed inward rectification quickly (Fig. 11A–C), others more slowly. At the end of the hyperpolarizing current pulse, sodium-dependent anode-break spikes were observed most of the time in onset neurons (Fig. 11A) and riding on top of the rebound response

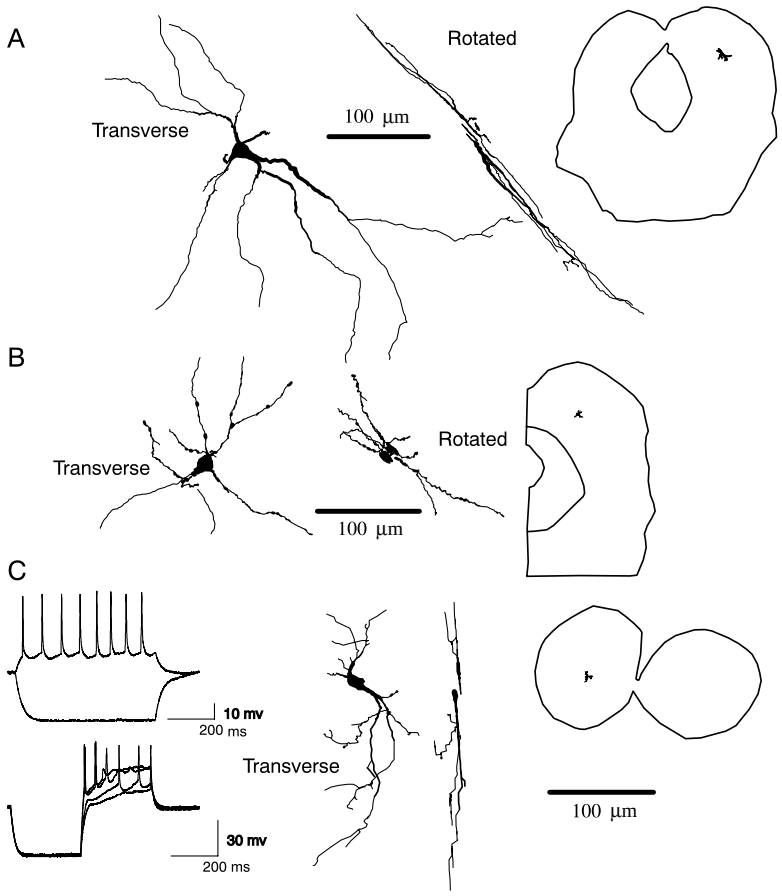

Fig. 5. Examples of buildup–pauser neurons. (A) Neurobiotin-filled large neuron, oriented in parallel to laminae in central nucleus (28 days old). Rotated view shows flat dendritic field (35 μm). (B) Neurobiotin-filled smaller oriented neuron with flat field (50 μm) at a more rostral level (29 days old). A few swellings on the dendrites were probably *post mortem* changes since no pathology was evident in the recordings from this neuron (see Fig. 4). (C) Lucifer Yellow-filled neuron with rostro-caudal orientation at border of central nucleus and dorsal cortex (11 days old). Rotated view shows flat dendritic field (30 μm). Insert shows sustained response to long current and buildup–pauser response after prehyperpolarization. Plane of section in C is similar to stereotaxic frontal plane; plane in A, B is tilted 20–30° caudal.

in rebound neurons (Fig. 11B). Anode-break spikes occurred less often in buildup–pauser units (Fig. 11C). An example of a buildup–pauser neuron that did have an anode-break spike is shown in Fig. 4A (recorded with sharp electrode).

Current–voltage relationships of IC neurons were examined with patch electrodes in normal saline (Fig. 12, left column) and in the presence of TTX to block sodium-dependent action potentials (Fig. 12, middle column). Neurons with onset discharges showed strong outward rectification during depolarizing current injections, both in normal saline and in the presence of TTX (Fig. 12, top; Fig. 13). For example, a small depolarizing current injection (e.g. 0 to 0.1 nA) resulted in a 30 mV change in membrane potential, from the resting potential of −60 mV to −30 mV (Fig. 12, top left and middle). However, a further increase in depolarizing current strength (from 0.1 to 0.5 nA) caused only a 12 mV increase in membrane potential (Fig. 12, top right). Even at high current strengths, the membrane potential of this onset cell did not increase beyond −10 mV. The range of potentials most sensitive to positive current injection is therefore 30 mV, between its resting membrane potential of −60 mV and −30 mV. Outward rectification continued to be present in TTX, and there was not much difference in the steady-state values of the *I–V* curves with and without TTX (Fig. 12, top right). This suggests that the presence of onset spikes do not affect the steady-state potential. In contrast to its outward rectification during depolarization, the steady-state response during hyperpolarization showed a response over a larger voltage range. An increase in current strength (from 0 to −0.2 nA) caused an 80 mV change in membrane potential (Fig. 12, top right).

Neurons with rebound discharges showed much less outward rectification than onset cells (Fig. 12, middle row; Fig. 13B). For example, an increase in depolarizing current strength from 0 to 0.5 nA depolarized the cell from its resting value of −50 mV to 0 mV (Fig. 12, middle left and center). Thus, this cell was sensitive over a greater range of positive currents than the onset cell. However, the range of voltages seen to hyperpolarizing currents was more limited than that seen in the onset cell. An increase in hyperpolarizing current strength from 0 to −0.2 nA in this cell caused only a 30 mV change in the steady-state membrane potential. As with onset cells, application of TTX did not alter the slope of the steady-state *I–V* function (Fig. 12, middle right).

Neurons with buildup–pauser discharges exhibited an outward rectification similar to that observed in onset cells (Fig. 12, bottom row; Fig. 13C). Typically, the potential range most sensitive to positive current injection was 30 mV, with an increase in current strength from 0 to 0.1 nA causing a shift in membrane potential from the resting value of −50 mV to −20 mV (Fig. 12, bottom right). Further increases in depolarizing current strength from 0.1 to 0.5 nA depolarized the

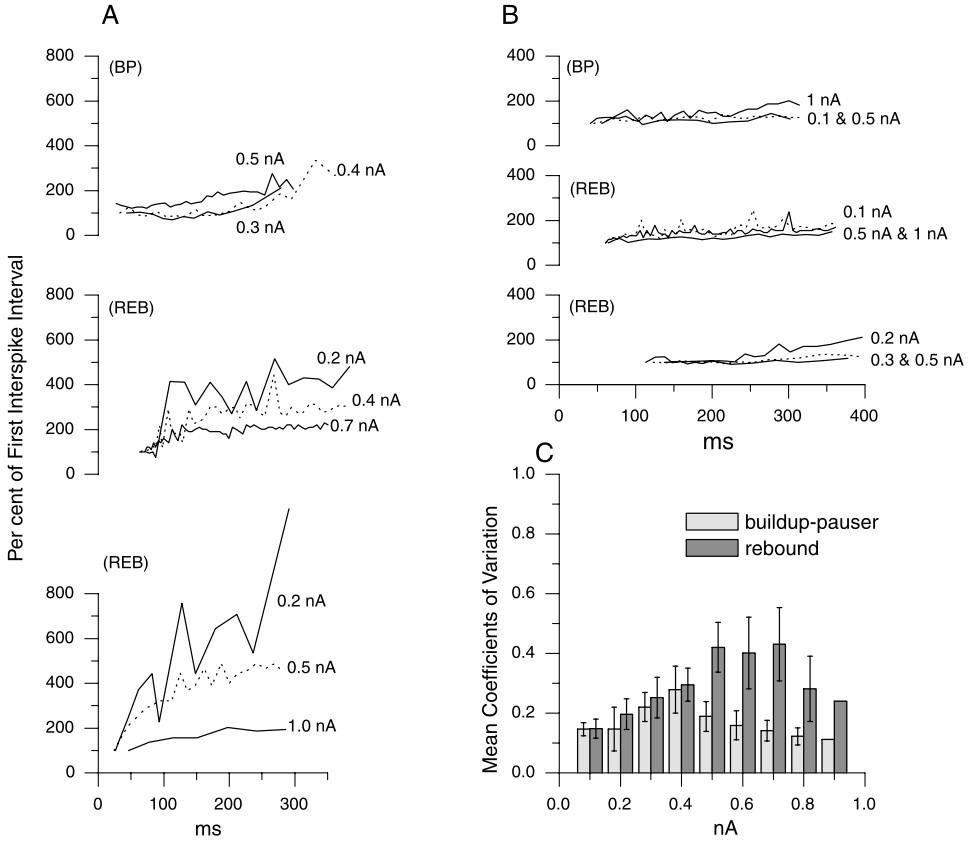

Fig. 6. Buildup–pauser and rebound neurons can be both adapting and regular, but buildup–pauser neurons tend to be more regular. (A) Plot of normalized interspike interval over time for adapting neurons. All interspike intervals are expressed as a percentage of the first interspike interval. Each trace represents the current level indicated. To qualify as adapting, subsequent interspike intervals are at least twice the duration of the first interspike interval. BP = buildup–pauser, REB = rebound. (B) For units classified as regular, the interspike interval remains relatively constant; no interspike interval reaches twice the first interspike interval. BP = buildup–pauser, REB = rebound. (C) Coefficients of variation show that buildup–pauser neurons tend to be more regular than rebound neurons ($n = 5$ buildup–pauser; $n = 7$ rebound neurons). Coefficient of variation was calculated for spikes generated by a single current pulse as the mean standard deviation divided by the mean interspike interval. Error bars = S.E. of the mean.

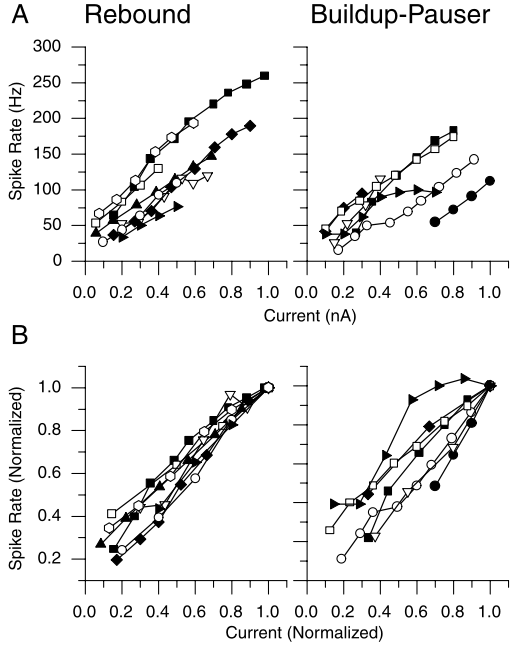

Fig. 7. Spike rate vs. current relationships for buildup–pauser and rebound neurons are linear and not significantly different. (A) Spike-rate per injected current for rebound and sustained buildup–pauser neurons. (B) The data in (A) normalized to the fastest spike rate and highest current level for each neuron.

cell to only −5 mV as a result of the outward rectification. In the hyperpolarizing direction, an injection of 0.2 nA of current hyperpolarized the membrane by 40 mV, which was similar to steady-state response of the rebound cell. As with the other neurons, blockage of sodium influx by TTX did not change the steady-state voltage responses dramatically.

The current–voltage relationships of neurons with the three discharge types were non-linear and differed in their input resistances. These input resistances were measured at steady-state and close to resting membrane potential (see Fig. 13, figure legend). Fig. 13 shows mean *I–V* curves obtained with patch electrodes in the presence of TTX. Neurons with onset discharges (Fig. 13, top) had the highest input resistances of 660 MΩ ($n = 6$). Neurons with rebound discharges (Fig. 13, middle) had the lowest input resistance, 111 MΩ ($n = 5$), and their *I–V* functions were the closest to linear. Neurons with buildup–pauser discharges (Fig. 13, bottom) had input resistances of 338 MΩ ($n = 5$).

DISCUSSION

The present brain slice experiments show that the membrane properties of IC neurons may be manifest as distinct electrophysiological responses. The largest class of

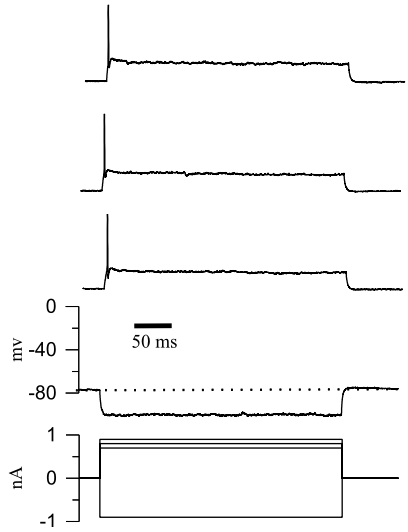

Fig. 8. Onset neurons (17/58 sharp electrodes, 14/41 patch electrodes) were different than sustained neurons in that they did not have a sustained action potential firing pattern. Onset neurons only fired one or two action potentials at the beginning of a depolarizing current injection.

IC neurons had sustained discharges, and subgroups of this class also exhibited either a rebound depolarization or a buildup–pauser discharge. Sustained neurons were either regular or adapting. A smaller class of IC neurons had onset discharges and was distinguished by a higher steady-state input resistance and the ability to entrain to higher frequency stimuli. The criteria for classifying cells as onset, buildup–pauser, or rebound are conspicuous, distinct, and non-overlapping, and they are correlated with distinctive current–voltage functions. These results suggest new categories for the classification of IC cell types based on the electrophysiological responses to current injection.

Previously, only small numbers of neurons in the central nucleus of the IC have been observed *in vitro*, and the classifications of the responses were too vague to encompass the diversity of responses seen in this study. Discharge patterns were reported for only 18 neurons in the central nucleus of the rat IC (two onset, two rapidly adapting, 14 sustained).[21] A preliminary report of the mouse also showed onset and sustained responses in the central nucleus.[58] These classifications were based in part on the amount of adaptation in the discharge pattern. In this study we have identified the onset unit, but used a number of different criteria to distinguish sustained cell types in the IC. For example, the rebound depolarization and the buildup–pauser responses were mutually exclusive and were used as distinguishing criteria in addition to adaptation. Neither the rebound discharge or the buildup–pauser discharge have been reported previously in the central nucleus of the IC.

Neuron types in the inferior colliculus

Electrophysiological responses to current suggest at least six cell types in the central nucleus of the IC. Onset neurons may represent a single cell type, while sustained neurons may include five different varieties based on different combinations of behaviors. Most sustained neurons exhibit either a rebound response or a buildup–pauser response. Both these types can show either adaptation (rebound-adapting or buildup–pauser-adapting) or regular, non-adaptive discharges (rebound-regular or buildup–pauser-regular). The last sustained neuron type has a sustained response but no buildup or rebound.

We have classified the buildup–pauser cells as a single group based on their response to a prehyperpolarizing stimulus, which causes a delay in the onset of the sustained firing. An identical prehyperpolarizing stimulus does not have the same effect in other IC neurons. This implies that some cells in the IC contain a current that is activated by the prehyperpolarization and that delays the onset of sustained firing. In other neurons, this current and the consequent buildup–pauser phenomenon is absent. Thus, we have place cells that exhibit the buildup–pauser phenomenon in a separate category. When a depolarizing stimulus is used without prehyperpolarization, buildup–pauser cells exhibit sustained firing without a delay similar to other sustained cells in the IC. In this respect, buildup–pauser cells do not differ from other sustained cells in the IC. However, buildup–pauser cells also show a consistently smaller amount of adaptation during their

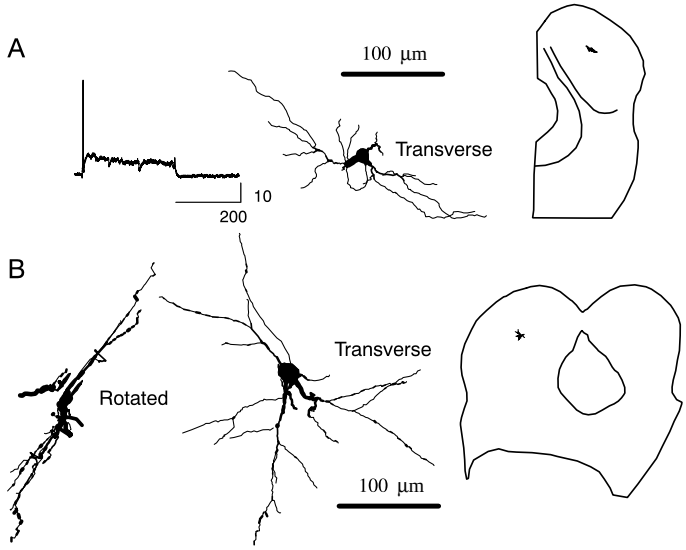

Fig. 9. Onset neurons filled with neurobiotin. (A) Onset response (left) in a medium-sized neuron, oriented in parallel to laminae in central nucleus (30 days old) with a flat dendritic field (40 μm). (B) Medium-sized neuron (18 days old) with flat field (65 μm).

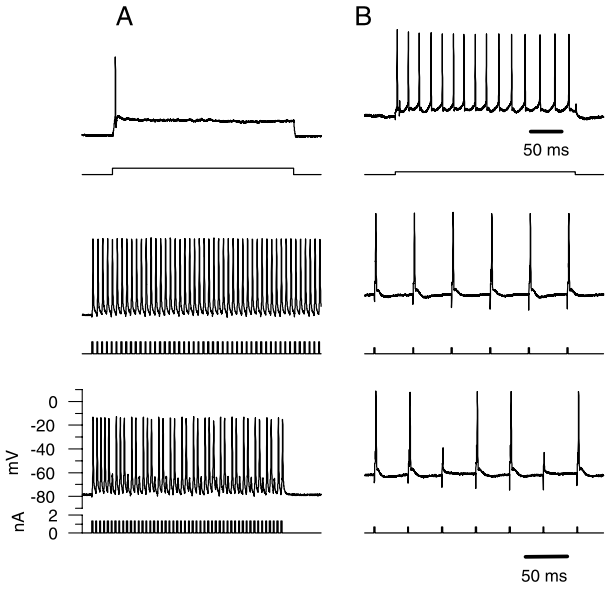

Fig. 10. Responses to trains of short current pulses. (A) An onset neuron responds to long duration depolarizing current with only one action potential (upper trace). Onset neurons can follow short intracellular current pulses at rates of 200 Hz (middle trace) and begin to fail at somewhat higher rates (lower trace: 250 Hz). (B) A rebound neuron (rebound not shown) can follow a train of current pulses at only a relatively low rate (middle trace, 25 Hz). The failure rate to a train of pulses (B, lower trace, 28 Hz) is low when compared to that of the onset neuron (A, lower trace).

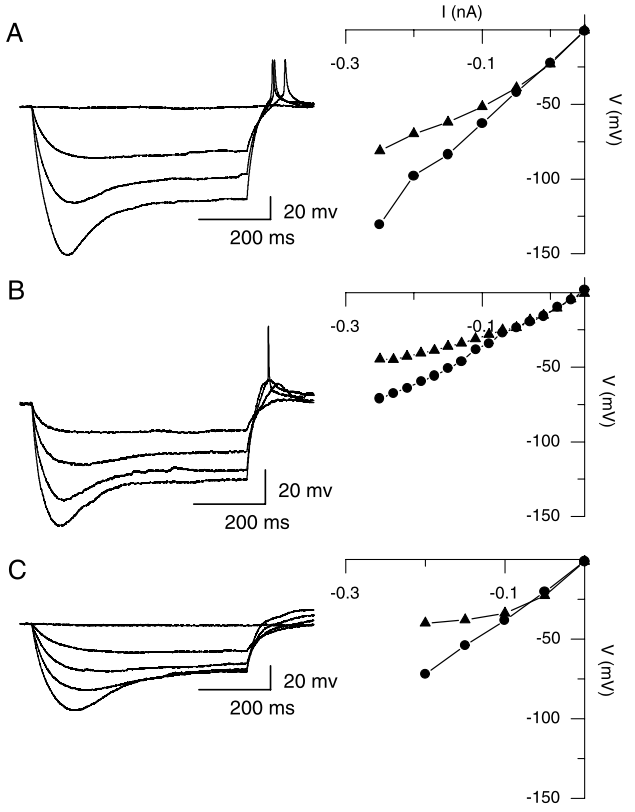

Fig. 11. Voltage responses of inferior colliculus neurons to hyperpolarizing current pulses. Current was injected into the soma through the recording electrode in the whole-cell patch configuration. (A) onset; (B) rebound; and (C) buildup–pauser neurons. Left panel: Voltage recordings. Steady-state values were measured 50 ms before the end of the step. Right panel: Instantaneous and steady-state current–voltage relationships for hyperpolarizing responses for the three cells shown in the left panel. Instantaneous values were measured 50 ms after the start of the current step in (A, B) and 100 ms after the start of the current step in (C). Inward rectification was assessed by comparison of current–voltage relationships immediately after the beginning of the response when it was maximal (right, circles) and the steady-state levels achieved later during the response (right, triangles).

sustained firing. Buildup–pauser cells therefore lie at the lower end of the adaptation continuum, with the highly adapting rebound cells at the opposite end. But, the buildup–pauser response to prehyperpolarization is unique and justifies their categorization as a separate class of cells.

The cell types suggested by the electrophysiological responses do not correspond to the previous binary morphological classifications in the central nucleus. In that nucleus, morphological studies have used the orientation or thickness of the dendritic tree to define cell type. In the cat, disc-shaped neurons have dendrites oriented in parallel to create fibrodendritic laminae, while stellate neurons are perpendicular to the laminae.[26,32,33,51,52] In the rat, the thickness of the dendritic tree, rather than the orientation is more diagnostic. Two neuron classes (flat and less-flat) are seen in adult rats, but both types parallel the laminae.[22] Even with the present small sample of well-filled neurons ($n = 26$), it is clear that the previously defined morphological types cannot be correlated with the electrophysiological response. Almost all well-labeled neurons had a dendritic field thickness of < 70 μm and would be classified as a disc-shaped, flat neuron. But, the flat/disc-shaped category contains unambiguous examples of each discharge pattern. Likewise, the finding of less-flat morphology for both onset and rebound cells in the central nucleus suggests that it is not unique to a single discharge pattern. Outside of the central nucleus, the stellate morphology was observed for all discharge types. It should be noted that the animals used in the present study were younger than the adult rats used to devise the flat/less-flat dichotomy. Perhaps more less-flat neurons would be seen in older animals.

Other morphological results are more suggestive and raise the possibility of a relationship between intrinsic electrophysiological properties and dendritic branching pattern. Buildup–pauser neurons may have simpler dendritic branching patterns than sustained or onset neurons. This observation is consistent with previous classification of stellate cells in the central nucleus based on simple or complex branching patterns.[33] It is also consistent with the present findings that neurons with these discharge patterns have a different input resistance. Different cell types in the IC defined by discharge pattern may have different passive dendritic electrotonic properties since those properties directly reflect input resistance and dendritic morphology (see for example Refs 43 and 44). Such speculations require the correlation of discharge pattern and branching patterns in more neurons. If electrophysiological types are distinguished by branching pattern, it may be a useful *in vitro* since the pattern and frequency of branching may be determined even if there is tissue distortion and an accurate three-dimensional reconstruction is not possible.

Different IC cell types may have different types of active conductances (voltage-gated or calcium-activated) that are activated when the neuron's voltage moves away from the resting potential. The present electrophysiological types are distinguished by different current–voltage relationships. For example, the onset neurons have outward

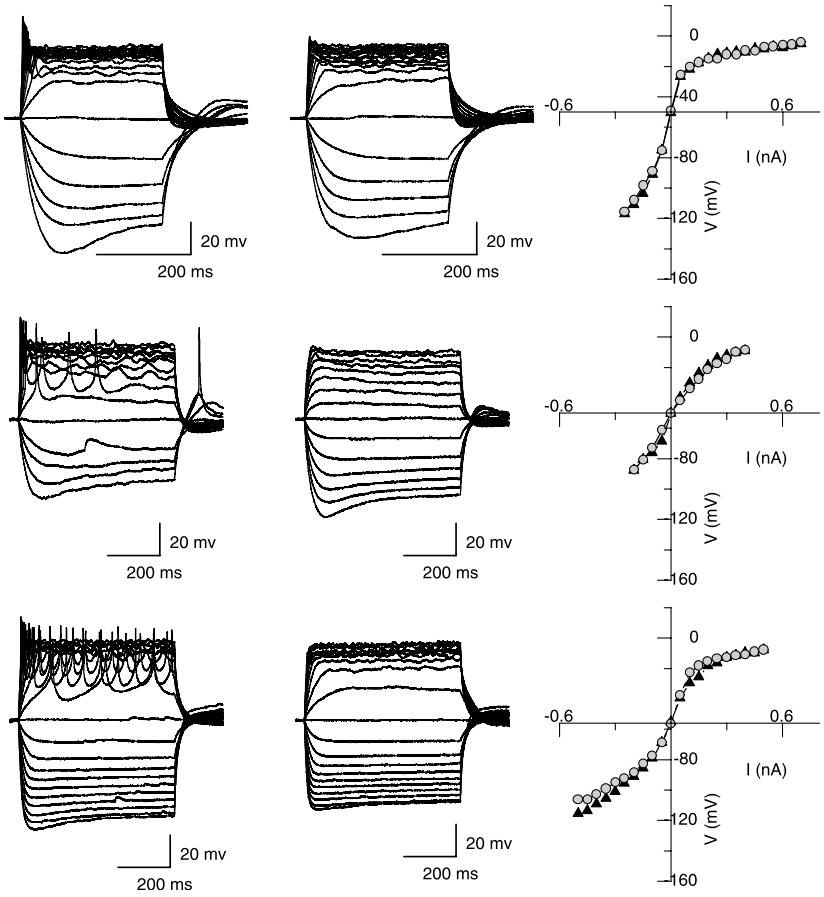

Fig. 12. Whole-cell current clamp recordings from inferior colliculus neurons in response to depolarizing and hyperpolarizing current steps in normal saline and in saline containing 2 μM TTX. Top row: onset neuron; resting potential = −50 mV. Middle row: rebound neuron; resting potential = − 50 mV. Bottom row: buildup–pauser neuron; resting potential = −56 mV. Left column: voltage changes in normal saline; middle column: voltages in TTX; right column: steady-state current-voltage relationships for each of the three cells in normal saline and in TTX. Steady-state measurements of voltage were made 50 ms before the end of the current step. Triangles, normal saline; circles, TTX.

rectification to depolarization, while rebound neurons show little rectification. Furthermore, the onset cells had time constants that were faster in the depolarizing direction. This may indicate the mechanism of the onset response includes a rapid activation of conductance, similar to the situation in bushy cells of the ventral cochlear nucleus, where a low-threshold potassium conductance is present.[24] Similar evidence for specific K^+ currents has been found in the IC.[54]

In sustained neurons, other active conductances may be related to other specific types of K^+ currents. For example, A-currents underlie buildup–pauser neurons in the dorsal cochlear nucleus.[14,15,24] It is highly likely that the buildup–pauser neurons in the IC also contain an A-current[54] while other types of sustained neurons do not. The A-current in the IC buildup–pauser neuron may contribute to a buildup or pauser response after it is deinactivated by inhibitory synaptic potentials that commonly lead excitatory potentials in the IC[18] or by the larger after-hyperpolarization seen in sustained neurons (present results). The stimuli used for prehyperpolarization in this study were comparable in amplitude but longer than inhibitory postsynaptic potentials observed *in vivo*.[18,37] Examples of specific K^+ currents in the IC are consistent with morphological studies that show many K^+ channel subunits are present in the IC but are restricted to subsets of neurons.[34,38]

Temporal coding versus signal transformations in the inferior colliculus

Our present results in the IC parallel findings in the auditory brainstem. An onset discharge pattern to current *in vitro* is seen in bushy and octopus cells in the cochlear nucleus, principle cells in the medial nucleus of the trapezoid body, and type 2 neurons in the ventral nucleus of the lateral lemniscus.[5,8,10,24,27,28,60,61] In some cells, these membrane properties are correlated with the ability to follow trains of synaptic stimuli.[5,28] *In vivo,* the bushy cell exhibits phase locking to low-frequency acoustic stimuli[8,49] and plays a key role in pathways devoted to processing interaural temporal differences (ITD) where phase locking is an important requirement.[56] In contrast, sustained firing to current *in vitro* is seen in stellate neurons in the cochlear nucleus[61] as is a regular response to acoustic stimuli *in vivo*.[4,8,49,62] Such responses may disrupt the faithful transmission of temporal information,[28] particularly above 1 kHz where their phase locking is diminished.[48] Moreover, stellate cells bypass the ITD centers of the superior olive and project directly to the IC.[31] Stellate cells may be more useful in energy detection than in temporal processing. Finally, the buildup–pauser pattern is seen in the fusiform cell both *in vitro* to current and *in vivo* to acoustic stimuli.[8,12,23,29,50] These cells in dorsal cochlear nucleus respond to frequencies above 2 kHz, where phase

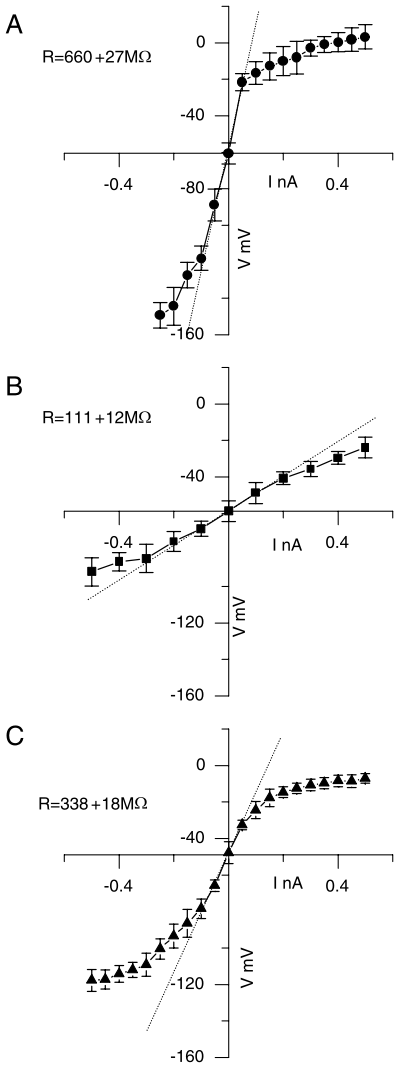

Fig. 13. Current–voltage relationships of the three cell types in the inferior colliculus obtained from whole-cell patch clamp recordings. (A) Onset, $n = 6$; (B) Rebound $n = 5$; and (C) Buildup–pauser neurons $n = 5$. The input resistance, R, was measured close to the end of the current injection and close to resting membrane potential (the slope of the linear portion of each curve passing through the origin), and is indicated by the dotted lines.

locking to pure tones is limited, and also project directly to the IC.[30]

As in the cochlear nucleus, the distinct discharge patterns reported here in the IC may signify neurons with different functions. The onset neurons follow trains of short current pulses. This response suggests that onset neurons may exhibit the best temporal coding in the IC. Onset neurons could correspond to the 25% of IC neurons that phase lock *in vivo*.[57] Phase locking is relatively poor in the IC compared to the lower auditory brainstem. In lower centers, phase locking extends to all frequencies required for ITD processing, while the upper limit in the IC is 600 Hz.[19,57] Poorer phase locking in the onset cells of the IC could be due to longer integration times required for synaptic inputs on highly branched dendrites. Integration may occur more rapidly in the cochlear nucleus and medial nucleus of the trapezoid body where it is aided by large, calyceal synaptic inputs on the cell bodies.

Sustained responses with temporal integration and a broad dynamic range may be the norm for the IC and suggest that most temporal processing has occurred at lower levels of the auditory system. The buildup–pauser and rebound neurons in the IC followed trains of short current pulses poorly. Both the rebound and buildup–pauser neurons have a broad dynamic range suggesting that firing frequency is not dependent on the temporal synchrony of the inputs. Maximal firing may occur when the neuron sums excitatory inputs both temporally and spatially. Some aspects of the sustained response may be modified depending on the integration of inhibitory and excitatory synapses. For example, the buildup–pauser IC neurons have the most regular firing and may "chop" or, instead, exhibit a buildup–pauser response depending on the level of inhibitory input.[20,46] In general, neurons with a sustained response may code stimulus intensity level and amplitude modulation at low modulation rates. Even the rebound, off-discharge may contribute to a response to amplitude-modulated stimuli under some conditions.[16] In contrast to onset neurons, the sustained cell types in the IC are more likely to transform their inputs into a rate code instead of a temporal code.

Acknowledgements—We thank Dr Philip Smith and Dr Paul Manis for their encouragement and generous advice during this project. Dr Lew Haberly, University of Wisconsin generously donated his custom software for data collection. Excellent technical assistance by Gretchen Beckius and Ta-Long Ju is greatly appreciated. Drs S. Kuwada, D. O. Kim, R. Batra, and D. Oertel provided useful comments on this work at earlier stages. We thank Dr Shu Hui Wu for reading the present paper and providing helpful comments. Preliminary results of this study have been reported in abstract form.[39–41,54] NIH Grant R01DC00189 (D.L.O.) supported this work.

REFERENCES

1. Adams J. C. (1981) Heavy metal intensification of DAB-based HRP reaction product. *J. Histochem. Cytochem.* **29,** 775.
2. Aghajanian G. K. and Rasmussen K. (1989) Intracellular studies in the facial nucleus illustrating a simple new method for obtaining viable motor neurons in adult rat brain slices. *Synapse* **3,** 331–338.
3. Banks M. I. and Smith P. H. (1992) Intracellular recordings from neurobiotin-labeled cells in brain slices of the rat medial nucleus of the trapezoid body. *J. Neurosci.* **12,** 2819–2837.
4. Blackburn C. C. and Sachs M. B. (1990) The representations of the steady-state vowel sound /e/ in the discharge patterns of cat anteroventral cochlear nucleus neurons. *J. Neurophysiol.* **63,** 1191–1212.
5. Brew H. M. and Forsythe I. D. (1995) Two voltage-dependent K + conductances with complementary functions in postsynaptic integration at a central auditory synapse. *J. Neurosci.* **15,** 8011–8022.
6. Davis K. A., Ramachandran R. and May B. J. (1999) Single-unit responses in the inferior colliculus of decerebrate cats II. Sensitivity to interaural level differences. *J. Neurophysiol.* **82,** 164–175.
7. Faye-Lund H. and Osen K. K. (1985) Anatomy of the inferior colliculus in rat. *Anat. Embryol.* **171,** 1–20.
8. Feng J. J., Kuwada S., Ostapoff E.-M., Batra R. and Morest D. K. (1994) A physiological and structural study of neuron types in the cochlear nucleus. I. Intracellular responses to acoustic stimulation and current injection. *J. comp. Neurol.* **346,** 1–18.
9. FitzPatrick K. A. (1975) Cellular architecture and topographic organization of the inferior colliculus of the squirrel monkey. *J. comp. Neurol.* **164,** 185–208.

10. Golding N. L., Robertson D. and Oertel D. (1995) Recordings from slices indicate that octopus cells of the cochlear nucleus detect coincident firing of auditory nerve fibers with temporal precision. *J. Neurosci.* **15,** 3138–3153.
11. Hamill O. P., Marty A., Neher E., Sakmann B. and Sigworth F. J. (1981) Improved patch-clamp techniques for high-resolution current recording from cells and cell-free membrane patches. *Pflügers Arch.* **391,** 85–100.
12. Hirsch J. A. and Oertel D. (1988) Intrinsic properties of neurones in the dorsal cochlear nucleus of mice, *in vitro*. *J. Physiol., Lond.* **396,** 535–548.
13. Irvine D. R. F. (1992) Physiology of the auditory brainstem. In *The Mammalian Auditory Pathway: Neurophysiology* (eds Popper A. N. and Fay R. R.), 1st edition, Vol. 1. Springer-Verlag, New York.
14. Kanold P. O. and Manis P. B. (1999) Transient potassium currents regulate the discharge patterns of dorsal cochlear nucleus pyramidal cells. *J. Neurosci.* **19,** 2195–2208.
15. Kim D. O., Ghoshal S., Khant S. L. and Parham K. (1994) A computational model with ionic conductances for the fusiform cell of the dorsal cochlear nucleus. *J. Acoust. Soc. Am.* **96,** 1501–1514.
16. Kuwada S. and Batra R. (1999) Coding of sound envelopes by inhibitory rebound in neurons of the superior olivary complex in the unanesthetized rabbit. *J. Neurosci.* **19,** 2273–2287.
17. Kuwada S., Batra R. and Stanford T. R. (1989) Monaural and binaural response properties of neurons in the inferior colliculus of the rabbit: effects of sodium pentobarbital. *J. Neurophysiol.* **61,** 269–282.
18. Kuwada S., Batra R., Yin T. C., Oliver D. L., Haberly L. B. and Stanford T. R. (1997) Intracellular recordings in response to monaural and binaural stimulation of neurons in the inferior colliculus of the cat. *J. Neurosci.* **17,** 7565–7581.
19. Kuwada S., Yin T. C. T., Syka J., Buunen T. J. F. and Wickesberg R. E. (1984) Binaural interaction in low-frequency neurons in inferior colliculus of the cat IV. Comparison of monaural and binaural response properties. *J. Neurophysiol.* **51,** 1306–1325.
20. Le Beau F. E. N., Rees A. and Malmierca M. S. (1996) Contribution of GABA- and glycine-mediated inhibition to the monaural temporal response properties of neurons in the inferior colliculus. *J. Neurophysiol.* **75,** 902–919.
21. Li Y., Evans M. S. and Faingold C. L. (1998) *In vitro* electrophysiology of neurons in subnuclei of rat inferior colliculus. *Hear. Res.* **121,** 1–10.
22. Malmierca M. S., Blackstad T. W., Osen K. K., Karagüelle T. and Molowny R. L. (1993) The central nucleus of the inferior colliculus in rat: A Golgi and computer reconstruction study of neuronal and laminar structure. *J. comp. Neurol.* **333,** 1–27.
23. Manis P. B. (1990) Membrane properties and discharge characteristics of guinea-pig dorsal cochlear nucleus neurons studied *in vitro*. *J. Neurosci.* **10,** 2338–2351.
24. Manis P. B. and Marx S. O. (1991) Outward currents in isolated ventral cochlear nucleus neurons. *J. Neurosci.* **11,** 2865–2880.
25. Meininger V., Pol D. and Derer P. (1986) The inferior colliculus of the mouse. A Nissl and Golgi study. *Neuroscience* **17,** 1159–1179.
26. Morest D. K. and Oliver D. L. (1984) The neuronal architecture of the inferior colliculus in the cat: Defining the functional anatomy of the auditory midbrain. *J. comp. Neurol.* **222,** 209–236.
27. Oertel D. (1983) Synaptic responses and electrical properties of cells in brain slices of the mouse anteroventral cochlear nucleus. *J. Neurosci.* **3,** 2043–2053.
28. Oertel D. (1985) Use of brain slices in the study of the auditory system: Spatial and temporal summation of synaptic inputs in cells in the anteroventral cochlear nucleus of the mouse. *J. Acoust. Soc. Am.* **78,** 328–333.
29. Oertel D. and Wu S. H. (1989) Morphology and physiology of cells in slice preparations of the dorsal cochlear nucleus of mice. *J. comp. Neurol.* **283,** 228–247.
30. Oliver D. L. (1984) Dorsal cochlear nucleus projections to the inferior colliculus in the cat: A light and electron microscopic study. *J. comp. Neurol.* **224,** 155–172.
31. Oliver D. L. (1987) Projections to the inferior colliculus from the anteroventral cochlear nucleus in the cat: Possible substrates for binaural interaction. *J. comp. Neurol.* **264,** 24–46.
32. Oliver D. L., Kuwada S., Yin T. C. T., Haberly L. and Henkel C. K. (1991) Dendritic and axonal morphology of HRP-injected neurons in the inferior colliculus of the cat. *J. comp. Neurol.* **303,** 75–100.
33. Oliver D. L. and Morest D. K. (1984) The central nucleus of the inferior colliculus in the cat. *J. comp. Neurol.* **222,** 237–264.
34. Oliver D. L. and Perney T. M. (1998) Potassium (K +) channel expression in the inferior colliculus (IC) of the rat. *Soc. Neurosci. Abstr.* **24,** 1882.
35. Ostapoff E.-M., Feng J. J. and Morest D. K. (1994) A physiological and structural study of neuron types in the cochlear nucleus. II. Neuron types and their structural correlation with response properties. *J. comp. Neurol.* **346,** 19–42.
36. Palombi P. S. and Caspary D. M. (1995) Response properties of CIC units of young adult Fischer 344 rats. *Assoc. Res. Otolaryngol. Abs.* **18,** 129.
37. Pedemonte M., Torterolo P. and Velluti R. A. (1997) *In vivo* intracellular characteristics of inferior colliculus neurons in guinea-pig. *Brain Res.* **759,** 24–31.
38. Perney T. M., Marshall J., Martin K. A., Hockfield S. and Kaczmarek L. K. (1992) Expression of the mRNAs for the KV3.1 potassium channel gene in the adult and developing rat brain. *J. Neurophysiol.* **68,** 756–766.
39. Peruzzi D. and Oliver D. L. (1994) Intracellular responses to current injections in slices of rat inferior colliclus (IC). *Soc. Neurosci. Abstr.* **20,** 321.
40. Peruzzi D. and Oliver D. L. (1997) Differential entraining capabilities of neurons in the rat inferior colliculus. *Assoc. Res. Otolaryngol. Abstr.* **20,** 190.
41. Peruzzi D., Shivaramakrishnan S. and Oliver D. L. (2000) Identification of cell types in brain slices of the inferior colliculus. *Assoc. Res. Otolaryngol. Abstr.* **23,** 256.
42. Pfeiffer R. R. (1966) Classification of response patterns of spike discharges for units in the cochlear nucleus: Tone burst stimulation. *Expl Brain Res.* **1,** 220–235.
43. Rall W. (1964) Theoretical significance of dendritic trees for neuronal input-output relations. In *Neuronal Theory and Modelling* (ed. Reiss R. F.). Stanford University, Stanford.
44. Rall W. (1967) Distinguishing theoretical synaptic potentials computed for different soma-dendritic distributions of synaptic input. *J. Neurophysiol.* **30,** 1138–1168.
45. Ramachandran R., Davis K. A. and May B. J. (1999) Single-unit responses in the inferior colliculus of decerebrate cats I. Classification based on frequency response maps. *J. Neurophysiol.* **82,** 152–163.
46. Rees A., Sarbaz A., Malmierca M. S. and Le Beau F. E. N. (1997) Regularity of firing of neurons in the inferior colliculus. *J. Neurophysiol.* **77,** 2945–2965.
47. Reyes A. D., Rubel E. W. and Spain W. J. (1994) Membrane properties underlying the firing of neurons in the avian cochlear nucleus. *J. Neurosci.* **14,** 5352–5364.
48. Rhode W. S. and Greenberg S. (1992) Physiology of the cochlear nuclei. In *The Mammalian Auditory Pathway: Neurophysiology* (eds Popper A. N. and Fay R. R.), 1st edition, Vol. 2. Springer-Verlag, NY.
49. Rhode W. S., Oertel D. and Smith P. H. (1983) Physiological response properties of cells labeled intracellularly with horseradish peroxidase in cat ventral cochlear nucleus. *J. comp. Neurol.* **213,** 448–463.
50. Rhode W. S., Smith P. H. and Oertel D. (1983) Physiological response properties of cells labeled intracellularly with horseradish peroxidase in cat dorsal cochlear nucleus. *J. comp. Neurol.* **213,** 426–447.
51. Rockel A. J. and Jones E. G. (1973) The neuronal organization of the inferior colliculus of the adult cat. I. The central nucleus. *J. comp. Neurol.* **147,** 22–60.
52. Rockel A. J. and Jones E. G. (1973) The neuronal organization of the inferior colliculus of the adult cat. II. The pericentral nucleus. *J. comp. Neurol.* **149,** 301–334.

53. Semple M. N. and Kitzes L. M. (1985) Single-unit responses in the inferior colliculus: different consequences of contralateral and ipsilateral auditory stimulation. *J. Neurophysiol.* **53,** 1467–1482.
54. Sivaramakrishnan S. and Oliver D. L. (1998) Ionic bases of response patterns of rat inferior colliculus neurons. *Soc. Neurosci. Abstr.* **24,** 1636.
55. Smith P. H. (1992) Anatomy and physiology of multipolar cells in the rat inferior collicular cortex using the *in vitro* brain slice technique. *J. Neurosci.* **12,** 3700–3715.
56. Smith P. H., Joris P. X. and Yin T. C. T. (1993) Projections of physiologically characterized spherical bushy cell axons from the cochlear nucleus of the cat: evidence for delay lines to the medial superior olive. *J. comp. Neurol.* **331,** 245–260.
57. Stanford T. R., Kuwada S. and Batra R. (1992) A comparison of the interaural time sensitivity of neurons in the inferior colliculus and thalamus of the unanesthetized rabbit. *J. Neurosci.* **12,** 3200–3216.
58. Wagner T. (1994) Intrinsic properties of identified neurones in the central nucleus of mouse inferior colliculus. *NeuroReport* **6,** 89–93.
59. Wisgirda M. E., Wang L.-Y. and Kaczmarek L. K. (1996) Characterization of potassium currents in the rat inferior colliulus using the *in vitro* brain slice. *Soc. Neurosci. Abstr.* **22,** 888.
60. Wu S. H. (1999) Physiological properties of neurons in the ventral nucleus of the lateral lemniscus of the rat: Intrinsic membrane properties and synaptic responses. *J. Neurophysiol.* **81,** 2862–2874.
61. Wu S. H. and Oertel D. (1984) Intracellular injection with horseradish peroxidase of physiologically characterized stellate and bushy cells in slices of mouse anteroventral cochlear nucleus. *J. Neurosci.* **4,** 1577–1588.
62. Young E. D., Robert J. M. and Shofner W. P. (1988) Regularity and latency of units in ventral cochlear nucleus: implications for unit classification and generation of response properties. *J. Neurophysiol.* **60,** 1–29.

(*Accepted* 15 *August* 2000)